

Vibrational analysis of the two non-equivalent, tetrahedral tungstate (WO_4) units in $\text{Ce}_2(\text{WO}_4)_3$ and $\text{La}_2(\text{WO}_4)_3$

Loyd J. Burcham, Israel E. Wachs *

Department of Chemical Engineering and Zettlemoyer Center for Surface Studies, Lehigh University, Bethlehem, PA 18015, USA

Received 17 September 1997; received in revised form 31 January 1998; accepted 31 January 1998

Abstract

The infrared and Raman spectra of $\text{Ce}_2(\text{WO}_4)_3$ and $\text{La}_2(\text{WO}_4)_3$, which are complicated by the superposition of bands from two non-equivalent WO_4 units, have been successfully assigned above 300 cm^{-1} according to T_d point group symmetry. Individual assignment of the two types of tungstate units, $\text{W}^{\text{I}}\text{O}_4$ (C_2 site symmetry) and $\text{W}^{\text{II}}\text{O}_4$ (C_1 site symmetry), relies on comparison with the spectra of tetrahedral reference tungstates of Na_2WO_4 , CaWO_4 , and MgWO_4 , and on the differences between $\text{W}^{\text{I}}\text{O}_4$ and $\text{W}^{\text{II}}\text{O}_4$ known from the crystal structure. Normal coordinate analysis indicates that the force constants for $\text{W}^{\text{I}}\text{O}_4$ and $\text{W}^{\text{II}}\text{O}_4$ roughly correlate with the amount of deviation from ideal T_d point symmetry, $\text{W}^{\text{I}}\text{O}_4$ being similar to CaWO_4 (both mildly distorted tetrahedrons), while $\text{W}^{\text{II}}\text{O}_4$ is closer to MgWO_4 (both highly distorted tetrahedrons). Non-ideality is also indicated by the calculated potential energy distribution (PED), which shows a substantial degree of vibrational interaction between bonds—especially in the less symmetric $\text{W}^{\text{II}}\text{O}_4$ unit. Frequency differences between IR and Raman bands that originate from the same T_d point group modes are attributed mainly to factor group splitting (i.e. Raman active *gerade* and IR active *ungerade* factor group modes). However, the LO-TO polarization mixing and surface modes that generate the observed vibrational frequencies in powders may also contribute to these frequency differences, since the magnitude of these effects may not be the same in Raman as in IR. Finally, it is likely that other rare earth tungstates of stoichiometry $\text{Ln}_2(\text{WO}_4)_3$, where $\text{Ln} = \text{La} \sim \text{Dy}$, have similar vibrational spectra due to their similar structures. © 1998 Elsevier Science B.V. All rights reserved.

Keywords: Infrared spectra; Raman spectra; Rare earth tungstates

1. Introduction

During recent catalytic studies [1], it became necessary to determine the infrared and Raman spectra of $\text{Ce}_2(\text{WO}_4)_3$ and $\text{La}_2(\text{WO}_4)_3$ for com-

parison with the Raman bands measured in $\text{CeO}_2/\text{WO}_3/\text{Al}_2\text{O}_3$ and $\text{La}_2\text{O}_3/\text{WO}_3/\text{Al}_2\text{O}_3$ catalysts. An extensive literature search revealed numerous vibrational studies on alkali rare earth tungstates [2–5], rare earth ordered perovskites [6–8], rare earth polytungstic acids [9,10], and rare earth halotungstates [11,12]. A few vibrational studies on pure rare earth tungstates were also found,

* Corresponding author. Tel.: +1 610 7583600; fax: +1 610 7586555.

including the measurement of the near-IR fluorescence spectra in $\text{La}_2(\text{WO}_4)_3$ [13], determination of periodic trends in the stretching modes of lanthanide tungstates [14], and the analysis of vibrational spectra in $\alpha\text{-Th}(\text{WO}_4)_2$ [15] and in Ln_2WO_6 ($\text{Ln} = \text{Sm}$, and rare earth-like Y and Bi) [16]. These studies, most of which concern tetrahedral WO_4 units [2–5,11,13–15], showed that the internal covalent vibrational modes in these WO_4 units can be successfully assigned based on tetrahedral, T_d , point group symmetry. However, very little vibrational information is available for the tetrahedrally coordinated $\text{Ce}_2(\text{WO}_4)_3$ and $\text{La}_2(\text{WO}_4)_3$. The objectives of this study, therefore, are firstly to report the vibrational spectra of these tungstates, and secondly to assign the internal covalent vibrational modes according to T_d point group symmetry.

Previous structural studies of $\text{Ce}_2(\text{WO}_4)_3$ and $\text{La}_2(\text{WO}_4)_3$ indicate that they are isomorphous with $\text{Eu}_2(\text{WO}_4)_3$ [17–23], for which the scheelite-like crystal structure was determined by Templeton and Zalkin [24]. This crystal structure determination showed that $\text{Eu}_2(\text{WO}_4)_3$ has C_{2h}^6 space group symmetry with four formula units per crystallographic unit cell. Additionally, tungsten resides on two different types of sites in which each W atom is surrounded by four oxygen atoms. One WO_4 unit, $\text{W}^{\text{I}}\text{O}_4$, is close to being a geometrically regular tetrahedron, with two bond lengths of 1.70 Å and two of 1.78 Å (averaging 1.74 Å). The other unit, $\text{W}^{\text{II}}\text{O}_4$, is a much more distorted tetrahedron with two bond lengths of 1.81 Å, one of 1.72 Å, and one of 1.77 Å (averaging 1.78 Å).

The assumption of tetrahedral, T_d , point group symmetry in the forthcoming internal mode analysis of the WO_4 units in $\text{Ce}_2(\text{WO}_4)_3$ and $\text{La}_2(\text{WO}_4)_3$ requires some justification. In their description of the isomorphous $\text{Eu}(\text{WO}_4)_3$ structure, Templeton and Zalkin [24] consider the two tungstate units (of C_2 and C_1 site symmetries, respectively, for $\text{W}^{\text{I}}\text{O}_4$ and $\text{W}^{\text{II}}\text{O}_4$) to be bridged as an irregular trigonal bipyramid with roughly D_{3h} point group symmetry. However, the Bravais cell does not contain an integer number of these D_{3h} point groups, making assignments based on the internal modes of these bipyramidal molecular

tungstate units meaningless. However, comparison of the IR and Raman spectra of $\text{Ce}_2(\text{WO}_4)_3$ and $\text{La}_2(\text{WO}_4)_3$ with the tetrahedral reference tungstates of Na_2WO_4 , CaWO_4 , and MgWO_4 , as well as with the previously cited tetrahedral rare earth tungstates [2–5,11,13–15], suggests that an approximation of T_d point group symmetry is not only appropriate, but also desirable because of the physical meaning which can be given to the internal T_d vibrations observed in the spectra. Therefore, the internal modes have been assigned by assuming tetrahedral, T_d , point group symmetry as an approximation of the actual, non-ideal symmetry of the WO_4 units.

2. Theoretical

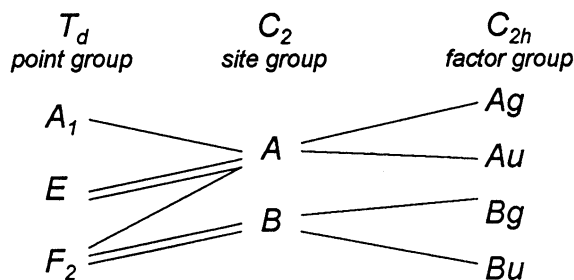
The representation for tetrahedral symmetry is [25]: $\Gamma_{T_d} = A_1(\nu_1) + E(\nu_2) + F_2(\nu_3) + F_2(\nu_4)$, in which all four vibrational modes are Raman active, but only the $F_2(\nu_3, \nu_4)$ modes are IR active. The $A_1(\nu_1)$ vibration is the symmetric stretch of the WO_4 unit, the $F_2(\nu_3)$ vibrations are the anti-symmetric stretches, and the $E(\nu_2)$ and $F_2(\nu_4)$ vibrations are bending modes. Since the site and factor groups of $\text{Ce}_2(\text{WO}_4)_3$ and $\text{La}_2(\text{WO}_4)_3$ are of lower symmetry than T_d , and the tetrahedral point groups themselves are non-ideal, the doubly-degenerate $E(\nu_2)$ and triply-degenerate $F_2(\nu_3, \nu_4)$ vibrations split into non-degenerate bands. For normal coordinate calculations the arithmetic average of these non-degenerate bands must be used, although in the past some investigators have used the theoretically less desirable intensity-weighted average [26].

Normal coordinate calculations were performed to refine the assignments and to estimate force constants (given in $\text{mdyn } \text{Å}^{-1}$). An algorithm was written in MATLAB[®] to allow calculations according to the GF matrix method. The principle of this method may be found in Nakamoto [25] and elsewhere, and the technique requires finding the solutions of the secular equation, $|\mathbf{GF} - \lambda\mathbf{I}| = 0$, where $\lambda = 4\pi^2c^2\nu^2$. The method of solution follows that of [27,28], involving a least-squares minimization of an eigenvalue-based variance. Force fields used in the calculations include the

three-constant Urey–Bradley Force Field (UBFF), the three-constant Orbital Valence Force Field (OVFF), and an approximated four-constant Generalized Valence Force Field (GVFF). For tetrahedral point group symmetry, the **G** and **F** matrix elements corresponding to these force fields, as well as a discussion of the physical meaning of the force constants, can be found in the excellent paper by Basile et al. [29]. In their study, Basile et al. found that the UBFF was generally superior for transition metal oxoanions like $(\text{WO}_4)^{2-}$, but that in some cases the OVFF was better (the GVFF has no degree of freedom and always fits the four observed frequencies exactly). Finally, in order to estimate the relative contribution of the force constants to the various normal modes, the potential energy distributions (PED's) were calculated as in [28], using the relationship $\text{PED} = \Lambda^{-1}(\text{JZ})\Phi$, where Λ and Φ are the diagonal matrices of eigenvalues and force constants, respectively, and (JZ) is the Jacobian matrix relating them.

Not surprisingly, the WO_4 internal T_d modes are also significantly influenced by the site and factor group symmetries of the crystal, so factor group analysis must be incorporated into the assignment process, as well. The previously cited crystal structure of $\text{Eu}_2(\text{WO}_4)_3$, which is isomorphous with $\text{Ce}_2(\text{WO}_4)_3$ and $\text{La}_2(\text{WO}_4)_3$, was used to perform the factor group analysis using the correlation method described by Fateley et al. for the Bravais cell [30]. For the C_{2h}^6 space group with four formula units per crystallographic unit cell there are only two formula units per Bravais cell, and the factor group is C_{2h} . The site symmetries of the atoms in the Bravais cell are as follows: 2 W^{I} (C_2), 4 W^{II} (C_1), 4 Ce (C_1), and 24 O (C_1). The WO_4 units were assumed to be centered on tungsten sites, and there are two $\text{W}^{\text{I}}\text{O}_4$ units and four $\text{W}^{\text{II}}\text{O}_4$ units in the Bravais cell. With this information the point group was correlated to the site and factor groups, and the results are summarized in Tables 1 and 2. After subtraction of the acoustic modes, which are inactive and have zero frequency (at wavevector $\mathbf{k} = 0$) in the Raman and IR spectra, the total representation for all vibrations, rotations, and

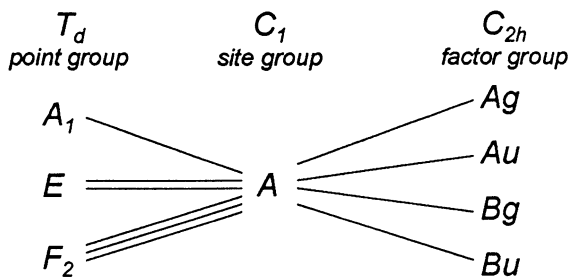
Table 1
Correlation table for $\text{W}^{\text{I}}\text{O}_4$ in $\text{Ce}_2(\text{WO}_4)_3$ and $\text{La}_2(\text{WO}_4)_3$



$$\Gamma_{\text{W}^{\text{I}}\text{O}_4} = 5 A_g + 5 A_u + 4 B_g + 4 B_u$$

translations in the crystal becomes: $\Gamma_{\text{total}} = 25 A_g + 24 A_u + 26 B_g + 24 B_u$. The 51 *gerade* modes are Raman active in the factor group, while the 48 *ungerade* modes are IR active. However, by considering only the nine (3n-6) internal vibrations in each type of WO_4 unit, there are a maximum of 18 Raman and 18 IR internal bands to be assigned in the spectra of $\text{Ce}_2(\text{WO}_4)_3$ and $\text{La}_2(\text{WO}_4)_3$ —half originating from $\text{W}^{\text{I}}\text{O}_4$ and half from $\text{W}^{\text{II}}\text{O}_4$.

Table 2
Correlation table for $\text{W}^{\text{II}}\text{O}_4$ in $\text{Ce}_2(\text{WO}_4)_3$ and $\text{La}_2(\text{WO}_4)_3$



$$\Gamma_{\text{W}^{\text{II}}\text{O}_4} = 9 A_g + 9 A_u + 9 B_g + 9 B_u$$

3. Experimental

The samples of $\text{Ce}_2(\text{WO}_4)_3$ and $\text{La}_2(\text{WO}_4)_3$ were prepared by first mixing stoichiometric amounts of ammonium *metatungstate* ($(\text{NH}_4)_6\text{H}_2\text{W}_{12}\text{O}_{40}$; Pfaltz and Bauer) with cerium(III) nitrate ($\text{Ce}(\text{NO}_3)_3 \cdot 6\text{H}_2\text{O}$; Johnson Matthey) and lanthanum nitrate ($\text{La}(\text{NO}_3)_3 \cdot 6\text{H}_2\text{O}$; Aldrich), respectively. The water soluble salt mixtures were then dissolved with distilled water in a crucible, and heated to a slow boil over a hotplate. The solutions were stirred continuously with a glass rod while the water was slowly evaporated. The crucibles and paste-like residues were then placed in a muffle furnace and heated to 900°C for 12 h. This temperature ensures complete reaction of the precursors to a single, homogeneous tungstate phase (Nassau et al. [17] has reported that these two tungstates form only a single, homogenous phase below 970°C). Finally, the crucibles were cooled to room temperature so that the samples could be ground (in the crucibles) with an agate pestle, followed by another 12 h of calcination at 900°C . The dissolution of the soluble precursors in water and the subsequent evaporation of the water are essential for producing a homogenous final compound. Attempts at a solid state reaction of well-mixed precursors in the solid phase resulted in WO_3 impurities in the final compounds, as measured by Raman spectroscopy.

In addition, Na_2WO_4 , CaWO_4 , and MgWO_4 were also prepared as reference compounds using ammonium *metatungstate* with stoichiometric amounts of 50% w/w NaOH solution (Fisher), calcium nitrate (Aldrich), and magnesium acetate (Johnson Matthey), respectively. The identities of the reference tungstates were confirmed by comparison of their measured Raman spectra with spectra reported in the literature [26;31–35]. X-ray diffraction was used to confirm the identities of the $\text{Ce}_2(\text{WO}_4)_3$ and $\text{La}_2(\text{WO}_4)_3$ samples. For the XRD experiments, a Philips APD 1700 Automated Powder Diffractometer was used with Cu-K α radiation of 45 kV and 30 mA. The powdered samples were scanned over 2θ from 10° to 70° at a rate of 3°min^{-1} . The resulting patterns matched those reported in the literature for both $\text{Ce}_2(\text{WO}_4)_3$ [21] and $\text{La}_2(\text{WO}_4)_3$ [17].

Raman spectra were recorded with a Triplemate spectrometer (Spex, Model 1877) coupled to an optical multichannel analyzer (Princeton Applied Research, Model 1463) equipped with an intensified photodiode array detector (cooled to -35°C). Samples were physically mixed with KBr and pressed into self-supporting wafers of ~ 150 mg. The sample wafers were then mounted on a sample rotator (Spex, Model 1445A), and the 514.5 nm line of an argon ion laser (Spectra Physics) was focused onto the spinning sample. Rotation of the sample reduces thermal broadening of the spectra from localized heating by the laser excitation source (15–40 mW at the sample). The ambient spectra were recorded as 25 signal averaged scans of 30 s each, with a resolution of approximately 2cm^{-1} .

Infrared spectra were recorded on a BioRad FTS-40A FTIR spectrometer by averaging 250 scans with a resolution of 2cm^{-1} . All spectra presented in the figures were taken in diffuse reflectance mode (DRIFTS), although some transmission spectra were also taken with samples mixed in KBr wafers. The optics used for the DRIFTS spectra were of the 'Praying Mantis' design (manf. by Graseby-Specac). Mid-IR spectra ($4000\text{--}400 \text{cm}^{-1}$; KBr beamsplitter) were obtained by diluting the samples in FTIR grade KBr powder (Alfa Aesar), while high density polyethylene powder (Polysciences, $20 \mu\text{m}$ particles) was used as the scattering diluent for collection of far-IR spectra ($500\text{--}100 \text{cm}^{-1}$; Mylar beamsplitter). The spectra were combined in the figures by scaling the data such that bands in the overlapping region ($500\text{--}400 \text{cm}^{-1}$) have the same intensity in both the mid- and far-IR. Also, some smoothing of the DRIFTS spectra was performed in order to enhance the signal to noise ratio.

4. Results

The Raman and IR spectra of $\text{Ce}_2(\text{WO}_4)_3$ and $\text{La}_2(\text{WO}_4)_3$ are given in Figs. 1 and 2, respectively. The Raman and IR spectra of reference tungstates Na_2WO_4 , CaWO_4 , and MgWO_4 are given in Figs. 3 and 4, respectively. The observed

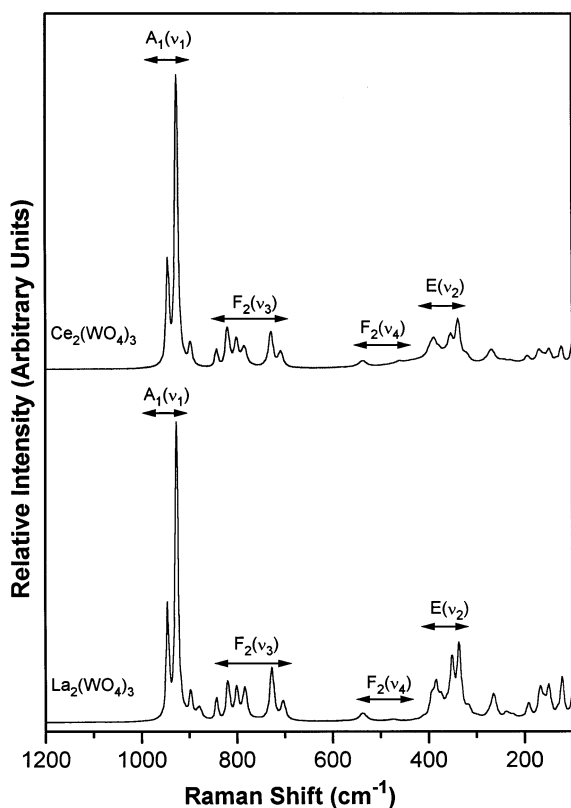


Fig. 1. Raman spectra of $\text{Ce}_2(\text{WO}_4)_3$ and $\text{La}_2(\text{WO}_4)_3$.

frequencies are also summarized in Tables 3 and 4. Note that there are bands in $\text{Ce}_2(\text{WO}_4)_3$, $\text{La}_2(\text{WO}_4)_3$, and MgWO_4 which are close to those measured for WO_3 (Alfa Aesar; Raman bands at 808, 714, 605, and 276 cm^{-1} , IR bands at 1057, 899, 876, 800, 620, 383, 337, 290, and 218 cm^{-1} ; see also Ref. [36]). However, the presence of WO_3 impurity can be ruled out in all of these samples based on some additional information. Firstly, in WO_3 the Raman band at 605 cm^{-1} and the IR bands at 1057 and 218 cm^{-1} , while rather weak, may be used as a fingerprint for the pure oxide because they do not overlap with any of the observed tungstate bands. These fingerprint bands do not appear in any of the tungstate spectra. Secondly, samples prepared with excess cerium and lanthanum precursors, which should react with all of the tungsten precursor, produced the same tungstate bands in the same relative intensities as those observed in the stoichiometric com-

pounds, although some important new bands were also observed in addition to the bands attributed to $\text{Ce}_2(\text{WO}_4)_3$ and $\text{La}_2(\text{WO}_4)_3$.

When $\text{Ce}_2(\text{WO}_4)_3$ was prepared in excess cerium precursor ($2\text{Ce}_2\text{O}_3 \cdot \text{WO}_3$) instead of the stoichiometric $\text{Ce}_2\text{O}_3 \cdot 3\text{WO}_3$, a new Raman band due to CeO_2 appeared at 467 cm^{-1} [36], new IR bands appeared at 856 and 694 cm^{-1} , and a slight increase was observed in the IR band at 936 cm^{-1} . The presence of CeO_2 suggests that all of the tungsten has been reacted. However, the appearance of new IR bands in conjunction with a relative increase in the 936 cm^{-1} IR band suggests that the new bands are due to a small amount of a different tungstate phase (probably $2\text{Ce}_2\text{O}_3 \cdot 9\text{WO}_3$ according to [21]). These same new bands appeared in samples formed in excess lanthanum ($2\text{La}_2\text{O}_3 \cdot \text{WO}_3$) and are also likely to

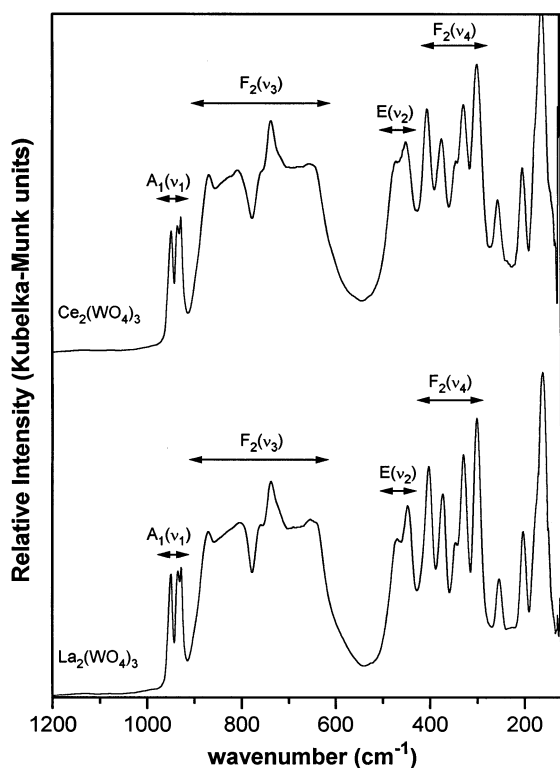


Fig. 2. Infrared spectra of $\text{Ce}_2(\text{WO}_4)_3$ and $\text{La}_2(\text{WO}_4)_3$. As is typical for the DRIFTS technique, intensities are expressed in Kubelka–Munk units to correct for diffuse reflectance distortions that would otherwise appear in the absorption spectra [37].

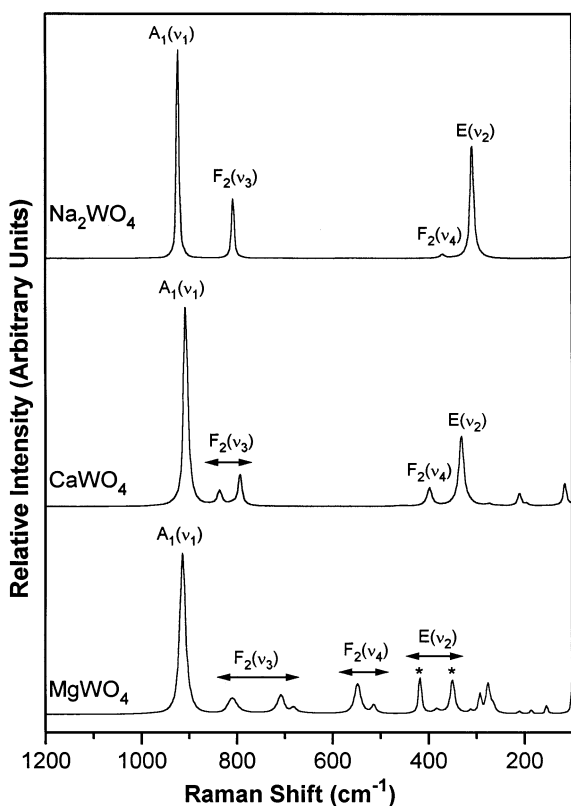


Fig. 3. Raman spectra of Na_2WO_4 , CaWO_4 , and MgWO_4 .

be due to a new $2\text{La}_2\text{O}_3 \cdot 9\text{WO}_3$ phase [22]. However, in addition to these new bands and bands from the stoichiometric $\text{La}_2(\text{WO}_4)_3$ phase, the excess lanthanum samples also exhibited very strong bands (Raman bands at 878, 793, 759, 729, and 414 cm^{-1} ; IR bands at 907, 849, 797, 751, 686, 610, 588, and 494 cm^{-1}) from a third phase that is probably either $\text{La}_6\text{WO}_{12}$ or $\text{La}_6\text{W}_2\text{O}_{15}$ according to published phase diagrams [22,23]. Nevertheless, the only traces of these different tungstate phases in the spectra of otherwise stoichiometric samples of $\text{Ce}_2(\text{WO}_4)_3$ and $\text{La}_2(\text{WO}_4)_3$ are the weak bands at 897 and 878 cm^{-1} in the Raman spectra (Fig. 1), and the band at 936 cm^{-1} in the IR spectra (Fig. 2). Thus, the spectra presented in Figs. 1 and 2 are essentially due to pure $\text{Ce}_2(\text{WO}_4)_3$ and $\text{La}_2(\text{WO}_4)_3$ —in agreement with the XRD data.

Regarding the infrared results, it was observed that when the sample was diluted in a scattering

medium like KBr or polyethylene, the DRIFTS spectra produced much sharper bands than the spectra obtained in transmission mode. This is most probably because scattering of the incident radiation by the transmission wafer interferes with the absorption signal in transmission mode, while in DRIFTS mode the measured changes in scattered radiation arise almost totally from sample absorption—suffering very little broadening from secondary effects. However, at high sample to diluent ratios the diffuse reflectance technique does suffer from the secondary effect of specular reflection. In practice, this means that the sample must be diluted and well-mixed in a scattering medium [37]. The degree of dilution is somewhat arbitrary, the requirement being that enough sample is present to generate a diffuse reflection spectrum but not so much as to cause specular

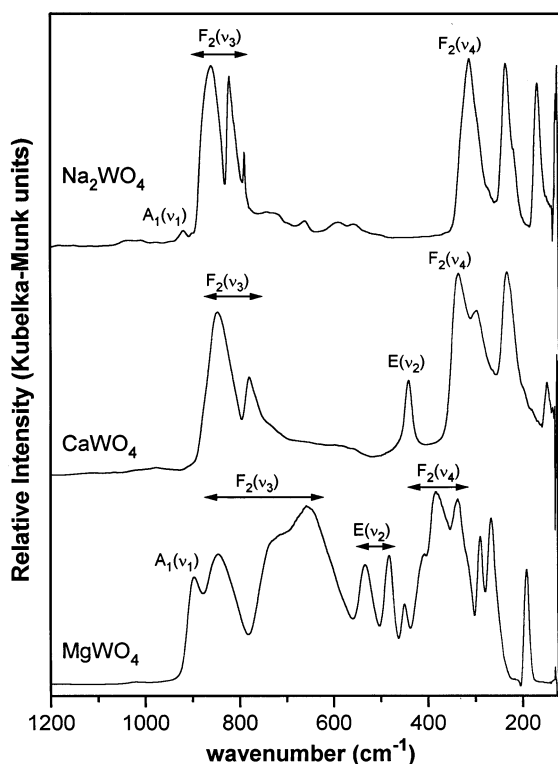


Fig. 4. Infrared spectra of Na_2WO_4 , CaWO_4 , and MgWO_4 . As is typical for the DRIFTS technique, intensities are expressed in Kubelka–Munk units to correct for diffuse reflectance distortions that would otherwise appear in the absorption spectra [37].

Table 3
Band frequencies (cm^{-1}) and assignments of reference tungstates

T_d pt. grp. assignments	Na_2WO_4		CaWO_4		MgWO_4	
	R	IR	R	IR	R	IR
$A_1(\nu_1)$	923 (s)	919 (w)	908 (s)	—	914 (s)	899 (m)
$F_2(\nu_3)$		860 (s)	836 (w)	847 (s)	810 (m)	845 (s)
$F_2(\nu_3)$	809 (m)	821 (s)	793 (m)	780 (m)	708 (m)	715 (s)
$F_2(\nu_3)$		790 (m)		682 (w)	657 (s)	
$E(\nu_2)$	304 (m)	—	330 (m)	442 (m)	416 (m)	534 (m)
$E(\nu_2)$					349 (m)	483 (m)
$F_2(\nu_4)$				334 (s)	549 (m)	408 (sh)
$F_2(\nu_4)$	370 (w)	311 (s)	398 (w)	296 (sh)	515 (w)	382 (s)
$F_2(\nu_4)$						338 (s)
External modes		232 (s)	273 (w)	233 (s)	313 (w)	291 (m)
		170 (s)	210 (w)	148 (w)	293 (m)	268 (s)
			116 (w)		277 (m)	194 (m)
					268 (sh)	
					212 (w)	
					187 (w)	
					155 (w)	

reflection. For all compounds studied in this investigation, mid- and far-IR DRIFTS spectra were taken over a range of dilution levels. Specular reflection peaks were identified as those which decreased relative to the other vibrational bands as the dilution was increased. The spectra taken for analysis were recorded at dilution levels in which the identified specular reflection bands were eliminated. Also, in the mid-IR it was possible to identify specular reflection bands by comparing the DRIFTS spectra to the corresponding transmission spectra, which have no such bands. Thus, the DRIFTS spectra presented in this paper are free from specular reflection bands.

5. Discussion

5.1. Band assignments

The vibrational spectra of the reference tungstates, summarized in Table 3, have been assigned previously by many authors [26,31–35]. While the Raman assignments for $E(\nu_2)$ and $F_2(\nu_4)$ were quite controversial in previous years

(see [33] for a review of the controversy), the detailed study by Weinstock et al. [38] on this issue demonstrated that $E(\nu_2)$ should always have a greater relative Raman intensity than $F_2(\nu_4)$. Modeling of the tungstate units in MgWO_4 with roughly T_d point group symmetry may seem questionable since Keeling [39] found the tungsten to be formally octahedrally coordinated based on the crystal structure. However, Blasse [34] has shown that MgWO_4 and other wolframite structures are better modeled as distorted tungstate tetrahedrons for the purposes of internal (covalent) band assignments, since two of the six W–O bonds are quite long and not likely to be very covalent in nature. The reference tungstates have been chosen so that splitting patterns in the idealized, degenerate T_d bands can be monitored as the actual point and site symmetries become less tetrahedral—i.e. from Na_2WO_4 (spinel with T_d point and site symmetry [26,31]) to CaWO_4 (scheelite with D_{2d} point and S_4 site symmetry [40]) to MgWO_4 (wolframite with less than D_{2d} point symmetry and C_2 site symmetry [39]) in order to compare a wide range of symmetries.

Assignment of the internal vibrational modes of $\text{Ce}_2(\text{WO}_4)_3$ and $\text{La}_2(\text{WO}_4)_3$ according to T_d point group symmetry requires consideration of the fact that their crystal structures indicate two distinct types of WO_4 tetrahedrons within the Bravais cell. Therefore, the spectra in Figs. 1 and 2 consist of two different sets of internal T_d vibrations superimposed onto one another, and these internal modes are generally assumed to occur above $\sim 300 \text{ cm}^{-1}$ [2]. From the factor group correlation tables, Tables 1 and 2, it is also apparent that both types of WO_4 tetrahedrons suffer a complete loss of degeneracy due to the low site and factor group symmetry of the crystal.

The factor group tables also indicate that, for W^{1}O_4 , all T_d point group vibrations are split into

either A_g and A_u or into B_g and B_u factor group modes, so that there is no splitting of non-degenerate bands within an individual Raman or IR spectrum. However, the W^{11}O_4 vibrations all split into A_g , A_u , B_g , and B_u factor group modes due to the low symmetry C_1 site group. Consequently, factor group (correlation) splitting of non-degenerate modes is possible [25,30], in which, for example, the A_1 point group vibration is split into two Raman bands (A_g and B_g) and two IR bands (A_u and B_u). It should also be acknowledged that the measured spectral bands are most properly assigned as A_g , A_u , B_g , and B_u factor group modes, and that the T_d point group assignments which will be given really refer to the types of vibrations from which these factor group modes

Table 4
Band frequencies (cm^{-1}) and assignments of $\text{Ce}_2(\text{WO}_4)_3$ and $\text{La}_2(\text{WO}_4)_3$

T_d pt. grp. assignments	$\text{Ce}_2(\text{WO}_4)_3$		$\text{La}_2(\text{WO}_4)_3$	
	R	IR	R	IR
$A_1(\nu_1); \text{W}^1\text{O}_4$	944 (s)	949 (m)	945 (s)	950 (m)
$A_1(\nu_1); \text{W}^{11}\text{O}_4$	925 (vs)	929 (m)	927 (vs)	928 (m)
New phase	897 (m)	936 (m)	897 (m)	935 (m)
New phase	—	—	878 (w)	—
$F_2(\nu_3); \text{W}^1\text{O}_4$	840 (m)	870 (s)	841 (m)	871 (s)
$F_2(\nu_3); \text{W}^{11}\text{O}_4$	818 (m)	825 (s)	818 (m)	823 (s)
$F_2(\nu_3); \text{W}^1\text{O}_4$	800 (m)	810 (s)	800 (m)	804 (s)
$F_2(\nu_3); \text{W}^1\text{O}_4$	784 (m)	756 (s)	783 (m)	760 (s)
$F_2(\nu_3); \text{W}^{11}\text{O}_4$	728 (m)	738 (s)	727 (m)	738 (s)
$F_2(\nu_3); \text{W}^{11}\text{O}_4$	707 (m)	656 (s)	703 (m)	655 (s)
$E(\nu_2); \text{W}^1\text{O}_4$	387 (m)	472 (s)	383 (m)	470 (m)
$E(\nu_2); \text{W}^{11}\text{O}_4$	352 (m)	451 (s)	349 (m)	447 (s)
$E(\nu_2); \text{W}^{11}\text{O}_4$	336 (m)	—	335 (m)	—
$F_2(\nu_4); \text{W}^1\text{O}_4$	—	405 (vs)	—	402 (vs)
$F_2(\nu_4); \text{W}^1\text{O}_4$	458 (w)	375 (s)	473 (w)	373 (s)
$F_2(\nu_4); \text{W}^1\text{O}_4$	—	—	—	—
$F_2(\nu_4); \text{W}^{11}\text{O}_4$	—	344 (sh)	—	345 (sh)
$F_2(\nu_4); \text{W}^1\text{O}_4$	536 (w)	329 (vs)	537 (w)	329 (vs)
$F_2(\nu_4); \text{W}^{11}\text{O}_4$	—	300 (vs)	—	301 (vs)
External modes	267 (m)	256 (m)	263 (m)	254 (m)
	192 (w)	204 (m)	237 (w)	203 (m)
	167 (w)	164 (vs)	224 (w)	160 (vs)
	146 (w)	—	191 (w)	—
	121 (w)	—	166 (m)	—
	—	—	148 (m)	—
	—	—	121 (m)	—

originate. Finally, while the discussion of band assignments will use the frequencies from $\text{Ce}_2(\text{WO}_4)_3$, the exact same arguments hold for the spectroscopically similar $\text{La}_2(\text{WO}_4)_3$.

From the $\text{Ce}_2(\text{WO}_4)_3$ Raman spectrum (Fig. 1), it is clear by comparison with the reference tungstates (Fig. 3) that the high frequency, intense bands at 944 and 925 cm^{-1} are due to the symmetric $A_1(\nu_1)$ vibrations of the two types of WO_4 units. The band at 944 cm^{-1} is assigned to $\text{W}^{\text{I}}\text{O}_4$ because the crystal structure indicates that this tetrahedron has the shortest average bond length and is, therefore, expected to vibrate at the highest frequency. Application of the bond length-stretching frequency correlation, developed by Hardcastle and Wachs [41], to this symmetric stretching mode yields the same conclusion. Also, the relative intensity of the $\text{W}^{\text{I}}\text{O}_4$ vibrations are expected to be less than those of $\text{W}^{\text{II}}\text{O}_4$ because there are only two $\text{W}^{\text{I}}\text{O}_4$ units in the Bravais cell, compared to four $\text{W}^{\text{II}}\text{O}_4$ units. However, conclusions based on relative Raman intensities must be made with caution because reflection intensities are generally non-linear with concentration and dependent on frequency. Nevertheless, the IR spectrum also shows that the 949 cm^{-1} band is lower in intensity than the 929 cm^{-1} band, although the difference is not as pronounced as in the Raman spectrum. The IR intensities for the $A_1(\nu_1)$ modes are much weaker than the $F_2(\nu_3, \nu_4)$ IR bands because ν_1 is IR inactive in pure T_d symmetry—the ν_1 modes appear in these spectra only because the WO_4 units are non-ideal in $\text{Ce}_2(\text{WO}_4)_3$. While factor group splitting cannot be ruled out as a possible origin for the 936 cm^{-1} IR band, the fact that the intensity of this band increases relative to the other $\text{Ce}_2(\text{WO}_4)_3$ bands in samples prepared with excess cerium suggests that this band is due to the secondary tungstate phase discussed previously. The Raman band corresponding to this minority phase appears at 897 cm^{-1} .

To assign the $F_2(\nu_3)$ bands in $\text{Ce}_2(\text{WO}_4)_3$, which appear in the region from 840 cm^{-1} to 707 cm^{-1} in the Raman spectrum and from 870 to 656 cm^{-1} in the IR spectrum, the splitting patterns of these bands in the reference tungstates must be examined in more detail. For example, the decay

of point and site group symmetry in the reference compounds splits the triply degenerate $F_2(\nu_3)$ vibrations into two Raman and two IR bands in CaWO_4 , and into three Raman and three IR bands in MgWO_4 . More importantly, notice that the high frequency ν_3 band in MgWO_4 is 102 cm^{-1} higher than the other two ν_3 bands in the Raman spectrum, and that it is 130 cm^{-1} higher in the IR spectrum. The other two lower frequency ν_3 bands are much closer together (separated by only 26 and 58 cm^{-1} in the Raman and IR spectra, respectively). The splitting of the $F_2(\nu_3)$ modes in $\text{Ce}_2(\text{WO}_4)_3$ is expected to follow a similar pattern. Therefore, the Raman bands at 840, 800, and 784 cm^{-1} (averaging 808 cm^{-1}) are assigned to the $F_2(\nu_3)$ vibrations in $\text{W}^{\text{I}}\text{O}_4$, and the Raman bands at 818, 728, and 707 cm^{-1} (averaging 751 cm^{-1}) are assigned to $\text{W}^{\text{II}}\text{O}_4$. The corresponding IR assignments are 870, 810, and 756 cm^{-1} (averaging 812 cm^{-1}) for $\text{W}^{\text{I}}\text{O}_4$, and 825, 738, and 656 cm^{-1} (averaging 740 cm^{-1}) for $\text{W}^{\text{II}}\text{O}_4$. This assignment is also consistent with the fact that $\text{W}^{\text{I}}\text{O}_4$ is expected to be somewhat less intense, and be at a higher average frequency, than $\text{W}^{\text{II}}\text{O}_4$.

The assignments for the $E(\nu_2)$ and $F_2(\nu_4)$ bending modes are simplified by observing that a frequency inversion relationship exists in the reference tungstates, in which $\nu_2(\text{IR}) \approx \nu_4(\text{R})$ and $\nu_4(\text{IR}) \approx \nu_2(\text{R})$. This relationship, which is due to factor group splitting, has been well known in tetrahedral tungstates and molybdates for some time [33]. In addition, $E(\nu_2)$ is more intense in the Raman than $F_2(\nu_4)$, whereas selection rules dictate that the reverse is true in the IR. Therefore, the Raman band at 387 cm^{-1} and the IR band at 472 cm^{-1} are assigned to $E(\nu_2)$ vibrations in $\text{W}^{\text{I}}\text{O}_4$, while the Raman bands at 352 and 336 cm^{-1} (averaging 344 cm^{-1}) and the IR band at 451 cm^{-1} are assigned to $E(\nu_2)$ vibrations in $\text{W}^{\text{II}}\text{O}_4$. Discrimination between the ν_2 bands of $\text{W}^{\text{I}}\text{O}_4$ and $\text{W}^{\text{II}}\text{O}_4$ is based on the higher frequencies and lower intensities of $\text{W}^{\text{I}}\text{O}_4$ relative to $\text{W}^{\text{II}}\text{O}_4$.

The assignment of the $F_2(\nu_4)$ bands to specific $\text{W}^{\text{I}}\text{O}_4$ or $\text{W}^{\text{II}}\text{O}_4$ units is more complicated and requires a closer examination of the splitting patterns in the reference tungstates. The IR spectra of the reference tungstates show that the $F_2(\nu_4)$

modes tend not to split as easily as the ν_3 vibrations (a trend also noted in [42]). This ‘clumping’ effect on the split ν_4 bands means that, compared to the ν_3 vibrations, there is more separation between the ν_4 bands of $\text{W}^{\text{I}}\text{O}_4$ and the ν_4 bands of $\text{W}^{\text{II}}\text{O}_4$. As before, the higher average frequencies and lower intensities of the IR bands at 405 and 375 cm^{-1} (averaging 390 cm^{-1}) indicate that they belong to the $\text{F}_2(\nu_4)$ vibrations in $\text{W}^{\text{I}}\text{O}_4$, while the IR bands at 344, 329, and 300 cm^{-1} (averaging 324 cm^{-1}) belong to the $\text{F}_2(\nu_4)$ vibrations in $\text{W}^{\text{II}}\text{O}_4$. Also notice that ν_4 is slightly more split in $\text{W}^{\text{II}}\text{O}_4$ because of the lower C_1 site symmetry (compared to the C_2 site symmetry of $\text{W}^{\text{I}}\text{O}_4$) and also because $\text{W}^{\text{II}}\text{O}_4$ has a more distorted point group symmetry than does the more ideally tetrahedral $\text{W}^{\text{I}}\text{O}_4$.

Finally, the Raman intensities for the $\text{F}_2(\nu_4)$ modes are too weak to display any observable splitting behavior, but these bands may still be assigned to $\text{W}^{\text{I}}\text{O}_4$ and $\text{W}^{\text{II}}\text{O}_4$ based on symmetry induced frequency shifts. In the reference tungstates, the Raman frequency of the ν_4 mode is higher than the ν_2 mode by only 66 and 68 cm^{-1} in Na_2WO_4 and CaWO_4 , respectively, but it is 160 cm^{-1} higher than ν_2 in less symmetric MgWO_4 . This suggests that, in the Raman spectrum, the ν_4 vibration for the generally lower frequency $\text{W}^{\text{II}}\text{O}_4$ is actually higher than the ν_4 vibration in $\text{W}^{\text{I}}\text{O}_4$ since $\text{W}^{\text{II}}\text{O}_4$ has less point and site group symmetry than $\text{W}^{\text{I}}\text{O}_4$. Indeed, the 536 cm^{-1} band in the Raman spectrum of $\text{Ce}_2(\text{WO}_4)_3$ is also more intense than the band at 458 cm^{-1} . Therefore, assignment of the band at 536 cm^{-1} to $\text{W}^{\text{II}}\text{O}_4$ is consistent with the fact that there is a higher population of $\text{W}^{\text{II}}\text{O}_4$ units in the Bravais cell.

In summary, the assignments for all bands in the infrared and Raman spectra of $\text{Ce}_2(\text{WO}_4)_3$ and $\text{La}_2(\text{WO}_4)_3$ are given in Table 4. Differences between the Raman and IR frequencies of bands originating from the same T_d point group modes are attributed primarily to factor group splitting (Tables 1 and 2) of these point group modes into Raman active *gerade* and IR active *ungerade* factor group modes (e.g. the frequency inversion of the bending modes, and the $A_1(\nu_1)$ mode of MgWO_4 vibrating at 914 cm^{-1} in Raman, but at 899 cm^{-1} in IR). However, for powders like those

used in the present study the observed vibrational intensity maxima are actually generated by the polarization mixing of longitudinal optic (LO) and transverse optic (TO) vibrations, which are often split in single crystals [43]. For example, Tarte et al. [33] found that the IR absorption maximum for the $\text{F}_2(\nu_3)$ T_d mode in CaWO_4 powder was intermediate between the single crystal LO and TO vibrations for this mode, although the exact frequency of this polarization-mixed mode varied by about 20 cm^{-1} depending on the particle size of the powder. Also, surface modes in the vicinity of the bulk polarization-mixed modes can shift the frequencies of the apparent intensity maxima of bands in vibrational spectra [43].

In the present study, the same particle size was used for both the Raman and IR measurements, so it is unlikely that particle size effects are responsible for the Raman and IR frequency differences of the same point group modes (also, the measured frequencies of the reference tungstates were very close to those reported in the literature for powdered samples). However, even for the same particle size it is possible that the surface modes and LO-TO polarization mixing may not behave identically in Raman as in IR. Hence, these effects cannot be ruled out as possible contributing sources to the Raman and IR frequency differences observed for the same T_d point group modes. Nevertheless, the factor group splitting is generally considered to be more significant [2,26]. Overall, the internal band assignments given in Table 4 are similar to previous T_d assignments for single WO_4 units in rare earth tungstates [2–5,11,15], but with the important distinction that in $\text{Ce}_2(\text{WO}_4)_3$ and $\text{La}_2(\text{WO}_4)_3$ there are two, non-equivalent tungstate units which have been separately assigned.

5.2. Normal coordinate analysis

Normal coordinate analysis provides additional insight into the vibrational nature of these tungstates, and has not appeared in the previous vibrational studies of tetrahedral rare earth tungstates [2–5,11,13–15]. The calculated frequencies and force constants for the three force fields used are shown in Table 5 for the reference

Table 5
Calculated frequencies (cm^{-1}) and force constants ($\text{mdyn } \text{\AA}^{-1}$) of reference tungstates^a

	Obs.	Calculated		
		UBFF	OVFF	GVFF
Na₂WO₄				
A ₁ (ν_1):	921	921	921	921
E(ν_2):	337 ^b	342	336	337
F ₂ (ν_3):	817	817	817	817
F ₂ (ν_4):	341	336	342	341
Variance:	—	1.22×10^{-4}	4.36×10^{-6}	N/A
Force constants:				$f_r = 6.21$
		$K = 4.78$	$K = 4.78$	$f_{rr} = 0.60$
		$F = 0.81$	$F = 0.81$	$f_x = 0.46$
		$H = 0.07$	$D = 0.17$	$f_{xx} = 0.05$
CaWO₄				
A ₁ (ν_1):	908	907	914	908
E(ν_2):	386	379	364	386
F ₂ (ν_3):	815	815	810	815
F ₂ (ν_4):	357	366	376	357
Variance:	—	3.02×10^{-4}	0.0021	N/A
Force constants				$f_r = 6.13$
		$K = 4.85$	$K = 4.69$	$f_{rr} = 0.55$
		$F = 0.73$	$F = 0.80$	$f_x = 0.50$
		$H = 0.18$	$D = 0.037$	$f_{xx} = 0.02$
MgWO₄				
A ₁ (ν_1):	907	904	906	907
E(ν_2):	446	464	448	446
F ₂ (ν_3):	736	740	737	736
F ₂ (ν_4):	454	434	452	454
Variance:	—	0.0017	1.93×10^{-5}	N/A
Force constants:				$f_r = 5.33$
		$K = 3.40$	$K = 3.31$	$f_{rr} = 0.81$
		$F = 1.08$	$F = 1.11$	$f_x = 0.81$
		$H = 0.28$	$D = 0.66$	$f_{xx} = 0.09$

^a Arithmetic averages were used for ν_2 , ν_3 , and ν_4 when these degenerate modes have been split into non-degenerate bands by lower symmetries in the crystals. Also, Raman and IR frequencies have been arithmetically averaged in order to estimate the frequencies of an 'effective' T_d point group.

^b For Na₂WO₄, the IR inactive E(ν_2) mode was taken to be 370 cm^{-1} based on the relationship $\nu_2(\text{IR}) \approx \nu_4(\text{R})$ [33]. Thus, in Table 5: $E(\nu_2) = 0.5 \cdot \{304 \text{ cm}^{-1} (\text{R}) + 370 \text{ cm}^{-1} (\text{IR})\} = 337 \text{ cm}^{-1}$.

compounds, and in Table 6 for Ce₂(WO₄)₃. The calculated values for La₂(WO₄)₃ have been omitted because of their similarity to those of Ce₂(WO₄)₃. The arithmetically averaged band positions were used to describe the degenerate T_d

modes which have been split by the lower symmetries of the crystal, and the Raman and IR frequencies have also been averaged to estimate the band positions of 'effective' T_d point groups.

For the reference tungstates, it is important to observe the trends in the force constants as the point and site symmetries are lowered. For instance, in highly symmetric Na₂WO₄ the magnitudes of the stretching force constants (K , K , and f_r in UBFF, OVFF, and GVFF, respectively) are 4–6 $\text{mdyn } \text{\AA}^{-1}$, whereas all of the other force constants are less than 1 $\text{mdyn } \text{\AA}^{-1}$. This indicates that the stretching vibrations in highly symmetric WO₄ units contain a significantly higher amount of potential energy than do the other modes. However, as the symmetry is lowered the stretching constants decrease. For the UBFF and OVFF, K decreases from 4.8 $\text{mdyn } \text{\AA}^{-1}$ in Na₂WO₄ to 3.4 $\text{mdyn } \text{\AA}^{-1}$ in MgWO₄. The f_r stretching constant in the GVFF also decreases from $\sim 6 \text{ mdyn } \text{\AA}^{-1}$ in Na₂WO₄ to $\sim 5 \text{ mdyn } \text{\AA}^{-1}$ in MgWO₄. Conversely, the force constants for bond angle deformation (H , D , and f_x in UBFF, OVFF, and GVFF, respectively) and bond interactions (the F repulsion constant in UBFF and OVFF; f_{rr} stretching and f_{xx} bending interaction constants in GVFF) are seen to increase as the point and site symmetries are lowered. Thus, the WO₄ units of lower symmetry are experiencing a withdrawal of potential energy away from the high energy stretching modes due to an increased amount of vibrational interaction between bonds.

For Ce₂(WO₄)₃, Table 6 shows that the stretching force constants for W^IO₄ are similar to those of CaWO₄, whereas the force constants for W^{II}O₄ are similar to those of MgWO₄. For example, the stretching force constants for W^IO₄ in Ce₂(WO₄)₃ are 4.4 (K , UBFF and OVFF), and 6.2 (f_r , GVFF) $\text{mdyn } \text{\AA}^{-1}$. The corresponding force constants for CaWO₄ are ~ 4.8 and $6.1 \text{ mdyn } \text{\AA}^{-1}$. The same stretching force constants for W^{II}O₄ in Ce₂(WO₄)₃ are 3.5 and $5.5 \text{ mdyn } \text{\AA}^{-1}$, compared to ~ 3.4 and $5.3 \text{ mdyn } \text{\AA}^{-1}$ in MgWO₄. This interesting correspondence is probably due to similarities in the amount of deviation exhibited by

these WO_4 units from ideal tetrahedral point symmetry: $\text{W}^{\text{I}}\text{O}_4$ and CaWO_4 have only mild distortion from T_d point symmetry compared to the much larger distortions in $\text{W}^{\text{II}}\text{O}_4$ and MgWO_4 . The bending and interaction constants are generally intermediate between those of CaWO_4 and MgWO_4 .

The potential energy distribution (PED) of $\text{Ce}_2(\text{WO}_4)_3$ is also presented in Table 7 for all three force fields. The PED shows a high degree of vibrational interaction between bonds, since even in the more symmetric $\text{W}^{\text{I}}\text{O}_4$ tetrahedron the $A_1(\nu_1)$ symmetric stretch has 48% contribution from the repulsion constant, F , in the UBFF and OVFF. The $\text{W}^{\text{II}}\text{O}_4$ symmetric stretch is 56% re-

pulsion in these two force fields, indicating much more interbond interaction due to the lower symmetry of this tetrahedron. The f_{rr} stretching interaction term in the GVFF also increases in the less symmetric $\text{W}^{\text{II}}\text{O}_4$ unit for the ν_1 mode. On the other hand, the $F_2(\nu_3)$ antisymmetric stretch appears to have greater stretching purity than ν_1 in all three force fields. The bending modes, $E(\nu_2)$ and $F_2(\nu_4)$, are also quite pure in the GVFF, but they have substantial repulsion (F) in the UBFF and OVFF. However, in all four modes and for all three force fields, the interaction terms are expectedly higher in the less symmetric $\text{W}^{\text{II}}\text{O}_4$. In general, the presence of significant vibrational interaction in these tungstate units is consistent with the fact that they are not perfect tetrahedrons—both $\text{W}^{\text{I}}\text{O}_4$ and $\text{W}^{\text{II}}\text{O}_4$ having varying degrees of deviation from ideal T_d point symmetry.

Table 6

Calculated frequencies (cm^{-1}) and force constants ($\text{mdyn } \text{\AA}^{-1}$) of $\text{Ce}_2(\text{WO}_4)_3^{\text{a}}$

$\text{Ce}_2(\text{WO}_4)_3$	Calculated			
	Obs.	UBFF	OVFF	GVFF
$\text{W}^{\text{I}}\text{O}_4$				
$A_1(\nu_1)$:	947	947	950	947
$E(\nu_2)$:	430	436	421	430
$F_2(\nu_3)$:	810	810	807	810
$F_2(\nu_4)$:	424	417	431	424
Variance:	—	2.21×10^{-4}	3.31×10^{-4}	N/A
Force constants:				
		$K = 4.46$	$K = 4.37$	$f_r = 6.24$
		$F = 1.00$	$F = 1.03$	$f_{\text{rr}} = 0.74$
		$H = 0.23$	$D = 0.53$	$f_x = 0.71$
				$f_{\text{xx}} = 0.06$
$\text{W}^{\text{II}}\text{O}_4$				
$A_1(\nu_1)$:	927	923	920	927
$E(\nu_2)$:	398	425	416	398
$F_2(\nu_3)$:	746	753	753	746
$F_2(\nu_4)$:	430	401	416	430
Variance:	—	0.0039	0.0015	N/A
Force constants:				
		$K = 3.49$	$K = 3.53$	$f_r = 5.52$
		$F = 1.14$	$F = 1.11$	$f_{\text{rr}} = 0.86$
		$H = 0.15$	$D = 0.40$	$f_x = 0.73$
				$f_{\text{xx}} = 0.12$

^a Arithmetic averages were used for ν_2 , ν_3 , and ν_4 when these degenerate modes have been split into non-degenerate bands by lower symmetries in the crystal. Also, Raman and IR frequencies have been arithmetically averaged in order to estimate the frequencies of an 'effective' T_d point group.

6. Conclusions

In conclusion, the infrared and Raman spectra of $\text{Ce}_2(\text{WO}_4)_3$ and $\text{La}_2(\text{WO}_4)_3$, which are complicated by the superposition of bands from two, non-equivalent WO_4 units, have been successfully assigned above 300 cm^{-1} according to T_d point group symmetry. Individual assignment of the two types of tungstate units, $\text{W}^{\text{I}}\text{O}_4$ (C_2 site symmetry) and $\text{W}^{\text{II}}\text{O}_4$ (C_1 site symmetry), has relied heavily on comparison with the tetrahedral reference tungstates of Na_2WO_4 , CaWO_4 , and MgWO_4 . This was especially true for the degenerate T_d bands, in which the reference tungstates were used to observe trends in the splitting patterns of these bands as the point and site symmetries became less tetrahedral. Assignment was also aided by the fact that $\text{W}^{\text{I}}\text{O}_4$ is expected to be somewhat less intense, and be at a higher average frequency, than $\text{W}^{\text{II}}\text{O}_4$ (there are only two $\text{W}^{\text{I}}\text{O}_4$ units in the Bravais cell, each with a relatively short average bond length, compared to the four $\text{W}^{\text{II}}\text{O}_4$ units with a longer average bond length).

Normal coordinate analysis indicates that the force constants for $\text{W}^{\text{I}}\text{O}_4$ and $\text{W}^{\text{II}}\text{O}_4$ roughly correlate with the amount of deviation from ideal

Table 7
Potential energy distribution (PED) for $\text{Ce}_2(\text{WO}_4)_3$ ^a

	Urey–Bradley force field			Orbital valence force field			Generalized valence force field			
	<i>F</i>	<i>H</i>	<i>K</i>	<i>F</i>	<i>D</i>	<i>K</i>	<i>f_r</i>	<i>f_{rr}</i>	<i>f_α</i>	<i>f_{αα}</i>
W^IO₄										
<i>v</i> ₁	0.47	0	0.53	0.49	0	0.51	0.74	0.26	0	0
<i>v</i> ₂	0.62	0.38	0	0.68	0.32	0	0	0	1.21	−0.22
<i>v</i> ₃	0.22	~0	0.78	0.23	~0	0.77	1.12	−0.13	0.01	0
<i>v</i> ₄	0.57	0.34	0.08	0.54	0.37	0.08	0.01	~0	0.99	0
W^{II}O₄										
<i>v</i> ₁	0.57	0	0.43	0.56	0	0.44	.68	0.32	0	0
<i>v</i> ₂	0.74	0.26	0	0.75	0.25	0	0	0	1.46	−0.46
<i>v</i> ₃	0.31	~0	0.69	0.30	~0	0.70	1.16	−.18	0.02	0
<i>v</i> ₄	0.62	0.24	0.14	0.57	0.30	0.13	0.02	~0	0.98	0

^a Table elements represent the fractional potential energy contribution of each force constant to each mode.

tetrahedral point symmetry: the force constants of W^IO₄ are similar to those of CaWO₄ (both are mildly distorted tetrahedrons), and W^{II}O₄ is closer to MgWO₄ (highly distorted tetrahedrons). It is possible that the site and factor groups may also have some influence on the calculated force constants due to the averaging procedure used to estimate the frequencies of the ‘effective’ *T_d* point groups in these tungstates. Non-ideality is also indicated by the calculated potential energy distribution (PED), which shows a substantial degree of vibrational interaction between bonds—especially in the less symmetric W^{II}O₄ unit.

Lastly, the influence of the factor group appears mainly as frequency differences between IR and Raman bands that have originated from the same *T_d* point group modes, since these point group modes have been split by the factor group into Raman active *gerade* and IR active *ungerade* factor group modes. Some contribution to these frequency shifts may also be due to the LO-TO polarization mixing and surface modes that generate the observed vibrational frequencies in powders, since the magnitude of these effects may not be the same in Raman as in IR. However, the factor group is usually considered to have the most significant splitting effect on the point group modes [2,26]. This factor group effect is most obvious for the bending modes, in which $\nu_2(\text{IR}) \approx \nu_4(\text{R})$ and $\nu_4(\text{IR}) \approx \nu_2(\text{R})$, but it also accounts for

frequency differences in the stretching modes (e.g. the *A₁*(*v*₁) mode of MgWO₄ vibrating at 914 cm^{−1} in Raman, but at 899 cm^{−1} in IR). Finally, it is likely that other rare earth tungstates of stoichiometry Ln₂(WO₄)₃, where Ln = La ~ Dy, have similar vibrational spectra due to their similar structures [17].

Acknowledgements

The authors gratefully acknowledge the United States Department of Energy — Basic Energy Sciences (DOE Grant # DEFG02-93ER14350) for financial support of this work.

References

- [1] (a) M.M. Ostromecki, L.J. Burcham, I.E. Wachs, N. Ramani, and J.G. Ekerdt, *J. Molec. Catal.*, in press (1998), (b) M.M. Ostromecki, L.J. Burcham, and I.E. Wachs, *J. Molec. Catal.*, in press (1998).
- [2] E.J. Baran, M.B. Vassallo, C. Cascales, P. Porcher, *J. Phys. Chem. Solids* 54 (1993) 1005.
- [3] J. Hanuza, *Acta Phys. Pol.* A70 (1986) 585.
- [4] K. Byrappa, A. Jain, *J. Mater. Res.* 11 (1996) 2869.
- [5] W.J. Schipper, G. Blasse, *Z. Naturforsch.* 29b (1974) 340.
- [6] (a) A.F. Corsmit, H.E. Hoefdraad, G. Blasse, *J. Inorg. Nucl. Chem.*, 34 (1972) 3401, (b) G. Blasse and A.F. Corsmit, *J. Solid State Chem.*, 6 (1973) 513. c) K.C. Bleijenberg and G. Blasse, *J. Solid State Chem.*, 17 (1976) 71.

- [7] A.N. Pandey, U.P. Verma, J.R. Chopra, *Indian J. Pure Appl. Phys.* 18 (1980) 510.
- [8] (a) H.J. Rother, A. Fadini, and S. Kemmler-Sack, *Z. Anorg. Allg. Chem.*, 463 (1980) 137, (b) H.J. Rother, S. Kemmler-Sack, U. Treiber, and W.R. Cyris, *Z. Anorg. Allg. Chem.*, 466 (1980) 131, (c) M. Herrmann and S. Kemmler-Sack, *Z. Anorg. Allg. Chem.*, 476 (1981) 115.
- [9] R. Shiozaki, E. Nishio, M. Morimoto, H. Kominami, M. Maekawa, Y. Kera, *Appl. Spectrosc.* 50 (1996) 541.
- [10] L. Chen, Y. Liu, Y. Chen, *J. Solid State Chem.* 68 (1987) 132.
- [11] L.H. Brixner, H.Y. Chen, C.M. Foris, *J. Solid State Chem.* 45 (1982) 80.
- [12] L.H. Brixner, H.Y. Chen, C.M. Foris, *J. Solid State Chem.* 44 (1982) 99.
- [13] X. Qi, Z. Luo, Q. Huang, J. Liang, J. Chen, Y. Huang, M. Qiu, H. Zhang, *Phys. Status Solidi A* 114 (1989) 127.
- [14] Y.M. Golutvin, K.S. Bagdasarov, E.A. Fedorov, E.G. Maslennikova, L.S. Strizhko, A.S. Popovich, L.G. Titov, *Sov. Phys. Crystallogr.* 28 (1983) 425.
- [15] M.S. Augsburg, J.C. Pedregosa, *J. Phys. Chem. Solids* 56 (1995) 1081.
- [16] J.H.G. Bode, H.R. Kuitj, M.A. Lahey, G. Blasse, *J. Solid State Chem.* 8 (1973) 114.
- [17] K. Nassau, H.J. Levinstein, G.M. Loiacono, *J. Phys. Chem. Solids* 26 (1965) 1805.
- [18] J.B. Nelson, J.H. McKee, *Nature* 158 (1946) 753.
- [19] L.H. Brixner, A.W. Sleight, *Mater. Res. Bull.* 8 (1973) 1269.
- [20] T. Gressling, H. Müller-Buschbaum, *Z. Naturforsch.* 50B (1995) 1513.
- [21] M. Yoshimura, F. Sibieude, A. Rouanet, M. Foex, *J. Solid State Chem.* 16 (1976) 219.
- [22] M. Yoshimura, A. Rouanet, *Mater. Res. Bull.* 11 (1976) 151.
- [23] G.I. Tyushevskaya, N.S. Afonskii, V.I. Spitsyn, *Dokl. Akad. Nauk SSSR* 170 (1966) 859.
- [24] D.H. Templeton, A. Zalkin, *Acta Crystallogr.* 16 (1963) 762.
- [25] K. Nakamoto, *Infrared and Raman Spectra of Inorganic and Coordination Compounds*, 4th edition, Wiley, New York, 1986.
- [26] R.H. Busey, O.L. Keller Jr., *J. Chem. Phys.* 41 (1964) 215.
- [27] D.E. Mann, T. Shimanouchi, J.H. Meal, L. Fano, *J. Chem. Phys.* 27 (1957) 43.
- [28] J. Overend, J.R. Scherer, *J. Chem. Phys.* 32 (1960) 1289.
- [29] L.J. Basile, J.R. Ferraro, P. LaBonville, M.C. Wall, *Coord. Chem. Rev.* 11 (1973) 21.
- [30] W.G. Fateley, F.R. Dollish, N.T. McDevitt, F.F. Bentley, *Infrared and Raman Selection Rules for Molecular and Lattice Vibrations: The Correlation Method*, Wiley, New York, 1972.
- [31] J.A. Horsley, I.E. Wachs, J.M. Brown, G.H. Via, F.D. Hardcastle, *J. Phys. Chem.* 91 (1987) 4014.
- [32] V.P. Mahadevan Pillai, T. Pradeep, M.J. Bushiri, R.S. Jayasree, V.U. Nayar, *Spectrochim. Acta* 53A (1997) 867.
- [33] (a) P. Tarte and M. Liegeois-Duyckaerts, *Spectrochim. Acta, Part A*, 28A (1972) 2029. (b) M. Liegeois-Duyckaerts and P. Tarte, *Spectrochim. Acta, Part A*, 28A (1972) 2037.
- [34] G. Blasse, *J. Inorg. Nucl. Chem.* 37 (1975) 97.
- [35] V.V. Fomichev, O.I. Kondratov, *Spectrochim. Acta, Part A* 50A (1994) 1113.
- [36] I.R. Beattie and T.R. Gilson, *J. Chem. Soc. A*, (1969) 2322.
- [37] J.M. Olinger, P.R. Griffiths, *Appl. Spectrosc.* 47 (1993) 687.
- [38] N. Weinstock, H. Schulze, A. Müller, *J. Chem. Phys.* 59 (1973) 5063.
- [39] R.O. Keeling Jr., *Acta Crystallogr.* 10 (1957) 209.
- [40] J.P. Russell, R. Loudon, *Proc. Phys. Soc.* 85 (1965) 1029.
- [41] F.D. Hardcastle, I.E. Wachs, *J. Raman Spectrosc.* 26 (1995) 397.
- [42] R.K. Khanna, E.R. Lippincott, *Spectrochim. Acta, Part A* 24A (1968) 905.
- [43] P.M.A. Sherwood, *Vibrational Spectroscopy of Solids*, Cambridge University Press, Cambridge, 1970.